Middle-East Journal of Scientific Research 16 (1): 73-87, 2013
ISSN 1990-9233
© IDOSI Publications, 2013
DOI: 10.5829/idosi.mejsr.2013.16.01.11622

Numerical Simulation of Strain Localization Using Mixed XFEM-Integral Type Nonlocal Model

M. Zarinfar and F. Kalantary

Department of Civil Engineering, K.N. Toosi University of Technology, Tehran, Iran

Abstract: If the modeling approach for strain localization with softening does not contain a material length-scale parameter, the numerical simulation suffers from the excessive mesh dependence. This paper presented the extended finite element (XFEM) method combined with new integral type nonlocal model for numerical simulation of strain localization with softening. The XFEM method was employed for simulation of high strain gradient in the localization band. The governing differential equations were regularized by nonlocal continuum theory, including the material length-scale parameter. For nonlocal plasticity, element size has a critical effect on the solution. Sufficiently refined meshes are required for an accurate solution without mesh dependency. It was shown that an extended finite element method can be applied to the problem to decrease the required mesh density close to the localization band. A new method based on the local bifurcation theory was proposed for the initiation and growth criterion of the strain localization interface. When using this method, the softening zone initiation locus did not need to be known in advance. Finally, several numerical examples were used to demonstrate the efficiency of the mixed XFEM–integral type nonlocal model in shear band localization modeling without mesh dependency.

Key words: XFEM · Integral type nonlocal model · Bifurcation · Strain localization

INTRODUCTION

Strain localization is of considerable interest because of its importance in the prediction of failure and residual bearing capacity for many engineering structures. It was mentioned in the literature that classical continuum mechanics cannot correctly predict strain localization and softening behavior. When localization or material softening occurs, the governing static equations lose elasticity or the governing dynamic equations lose hyperbolicity (onset of bifurcation) [1, 2]. Therefore, the boundary value problem becomes mathematically ill-posed, which results in mesh dependency. This inefficiency is due to the fact that classical continuum mechanics has no material length scale parameter [3]. As a result, by refining the mesh, the plastic strain is localized in a narrower region. To regularize the boundary value problem micro-polar models [4], higher-order gradient models [5], visco-plasticity [6] and integral-type nonlocal plasticity models [7] are commonly used.

The integral-type nonlocal model is based on the replacement of a certain variable by integral averaging. The first application of the integral-type nonlocal model into plasticity was made by Erigena [8, 9]. However, Erigena's formulation cannot be used as a localization limiter because the averaging operator was applied to the total strain tensor which could cause spurious instabilities (zero energy modes) [3]. Pijaudier-Cabot and Bazant [10] and Bazant and Lin [11] applied the nonlocal operator only to those parameters which control the softening process. Finite element implementation of nonlocal plasticity was presented by Stromberg and Ristinmaa [12], Brunig *et al*. [13], Maier [14, 15] and Tejchman [16]. Jirasek [17] presented an overview of the integral-type nonlocal model for damage and fracture, Bazant and Jirasek [18] did for plasticity and damage and Jirasek and Rolshoven [3] did for plasticity. In the present paper, a new relation is proposed to calculate the stress rate based on the integral-type nonlocal model. This relation depends on the local plastic strain rate and integral averaging of the local plastic strain rate.

Corresponding Author: M. Zarinfar, Department of Civil Engineering, K.N. Toosi University of Technology, Tehran, Iran.

The mathematical foundation of the XFEM was discussed by Melenk and Babuska [19]. The first application of XFEM to crack growth problems was done by Belytschko and Black [20]. The advantage of this technique is its independency of the crack geometry on the mesh. Fries and Belytschko [21] provided an overview of XFEM applications. This numerical technique has been used to simulate shear bands and strain localization [22-27]. In the context of the nonlocal model, the mesh must be sufficiently refined near the high strain gradient region to resolve mesh dependency. Adaptive mesh refinement can be used to overcome this, however, adaptivily may produce stress oscillations cause by the poor ability of approximation functions to capture the non-smooth pattern of strain near the softening zone [22, 28]. The XFEM method is an alternative that can be applied to decrease the required mesh density close to the shear band. This numerical strategy allows modeling of the mesh-independent approximation of the non-smooth solutions using enrichment functions which are close to the exact localization mode. In addition, the computational effort is reduced compared to remising methods.

Strain localization starts when the ellipticity conditions of the static equation or the hyperbolicity of the dynamic equation are lost (onset of bifurcation) [11, 29]. If the constitutive tensor is symmetric, this condition is equivalent to zero or the negative determinant of the acoustic tensor. Therefore, the singularity of the acoustic tensor was considered as the onset condition of strain localization (local bifurcation criterion) [30-34]. When using the local bifurcation theory and XFEM, the softening zone initiation locus does not need to be known in advance. Strain localization begins at the first point in which the local criterion of bifurcation is satisfied (singularity of acoustic tensor). Moreover, the strain localization interface progresses are obtained independently from the mesh. With continued loading, local criterion of bifurcation is satisfied in more points and thereafter strain localization grows inside the body.

In the present paper, use of XFEM combined with an integral-type nonlocal continuum model is proposed for the simulation of the strain localization in elasto-plastic solids. The XFEM formulation is presented in the framework of a generalized continuum model based on the nonlocal continuum theory, including the material length-scale parameter. The standard FE approximation is enriched by employing additional terms based on the hyperbolic tangent function. This function is continuous and differentiable and can model high strain gradient. The interfaces of the localization band are represented independently of the element boundaries by XFEM. Local bifurcation is considered as a criterion for the initiation and growth of the strain localization interface. Finally, several numerical examples are used to demonstrate the efficiency of the mixed XFEM–integral type nonlocal model in shear band localization modeling without mesh dependency.

XFEM Formulation of Elasto-Plastic Solids: The governing equation in an updated Lagrangian framework is a linear momentum balance equation.

$$\mathrm{div}\sigma - \rho\ddot{u} + \rho\mathbf{b} = 0 \tag{1}$$

where σ is the stress, b refers to the body force and ρ is the density. The Dirichlet boundary condition is $\mathbf{u} = \bar{\mathbf{u}}$ on $\Gamma=\Gamma_u$. The Neumann boundary conditions is $\mathbf{t} = \boldsymbol{\sigma}\mathbf{n}$ on $\Gamma=\Gamma_t$.

The spatial discretization involving the variables u is achieved by suitable shape functions. Therefore, the finite element polynomial displacement field is enriched with regular Heaviside function which models the high displacement gradient in the localization band. The approximation of displacement (u) can be expressed in the following form:

$$\mathbf{u}_{(\mathbf{x},t)} = \sum_{I=1}^{n^u_{nod}} N^u_{i(\mathbf{x})}\bar{\mathbf{u}}_{i(t)} + \sum_{I=1}^{n^u_{nod}} N^u_{i(\mathbf{x})Enr}\bar{\mathbf{a}}_{i(t)} \tag{2}$$

$$N^u_{i(\mathbf{x})Enr} = N^u_{i(\mathbf{x})}\left(R_{(\mathbf{x})}[?_{(f(\mathbf{x}))} - ?_{(f(\mathbf{x}_i))}]\bar{\mathbf{a}}_{i(t)}\right)$$

where n^u_{nod} denotes the number of element nodes, N^u_i the standard finite element shape function associated with node i, $\bar{\mathbf{u}}_i$ the standard nodal displacement, $\bar{\mathbf{a}}_i$ the additional degrees of freedom (DOF) associated with node i. In the above relation, $\psi_{(\mathrm{x})}$ denotes the appropriate enrichment function and $\varphi(\mathrm{x})$ is the distance from the strain localization interface. $R_{(\mathrm{x})}$ is the ramp function which resolves difficulties in blending elements [21].

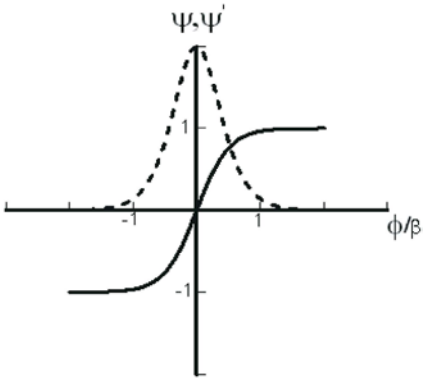

Fig. 1: The smoothed hyperbolic tangent function and its derivative

$$R_{(\mathbf{x})} = \sum_{i}^{n_{enr}} N_{i(\mathbf{x})} \tag{3}$$

where n_{ear} is the number of enriched nodes of the element. This numerical technique improves the description of the displacement field inside the localized zone by adding the special enrichment functions which can model high gradient of displacement field. These functions and their gradients must be similar to the profile of displacement and strain fields. In this study, the hyperbolic tangent is employed to describe the corresponding profiles, as shown in Fig. 1. This function is defined as:

$$\psi_{\varphi(x)} = tanh(2\varphi(\mathbf{x})/\beta) \tag{4}$$

where β is the parameter which controls width of the shear band. By selecting several values of β, one can construct a series of enrichment functions describing the displacement profile near the strain localization interface. By substituting equation (2) in to strain rate definition, strain matrix can be defined as:

$$\dot{\varepsilon} = \sum_{i=1}^{n_{nod}^{u}} \begin{bmatrix} \mathbf{B}_{i(\mathbf{x})} & \mathbf{B}_{i(\mathbf{x})Enr} \end{bmatrix} \begin{bmatrix} \dot{\overline{u}}_{i(t)} \\ \dot{\overline{a}}_{i(t)} \end{bmatrix} \tag{5}$$

in which

$$B_{i(x)} = \begin{bmatrix} \frac{\partial N_{i(x)}^{u}}{\partial x_1} & 0 \\ 0 & \frac{\partial N_{i(x)}^{u}}{\partial x_2} \\ \frac{\partial N_{i(x)}^{u}}{\partial x_2} & \frac{\partial N_{i(x)}^{u}}{\partial x_1} \end{bmatrix} \quad B_{i(x)Enr} = \begin{bmatrix} \frac{\partial N_{i(x)Enr}^{u}}{\partial x_1} & 0 \\ 0 & \frac{\partial N_{i(x)Enr}^{u}}{\partial x_2} \\ \frac{\partial N_{i(x)Enr}^{u}}{\partial x_2} & \frac{\partial N_{i(x)Enr}^{u}}{\partial x_1} \end{bmatrix} \tag{6}$$

To obtain the weak form of the governing equations, Galerkin's procedure is used. The test functions $\delta u(\mathbf{x}, t)$ which has the same form as $\mathbf{u}$ is multiplied by equations (1) and integrated over the domain Ω. Using the Divergence theorem leads to the following equation as:

$$M\begin{bmatrix} \ddot{\overline{u}} \\ \ddot{\overline{a}} \end{bmatrix} + \int_{\Omega} B^{T}\sigma d\Omega - F = 0 \tag{7}$$

in which

$$M = \begin{bmatrix} \int_{\Omega}(N^{u})^{T}\rho N^{u} d\Omega & \int_{\Omega}(N^{u})^{T}\rho N_{Enr}^{u} d\Omega \\ \int_{\Omega}(N_{Enr}^{u})^{T}\rho N^{u} d\Omega & \int_{\Omega}(N_{Enr}^{u})^{T}\rho N_{Enr}^{u} d\Omega \end{bmatrix} \tag{8}$$

$$F = \begin{bmatrix} \int_{\Omega}(N^{u})^{T}\rho b d\Omega + \int_{\Gamma_t}(N^{u})^{T}\overline{t} d\Gamma \\ \int_{\Omega}(N_{Enr}^{u})^{T}\rho b d\Omega + \int_{\Gamma_t}(N_{Enr}^{u})^{T}\overline{t} d\Gamma \end{bmatrix} \tag{9}$$

The governing equations (7) are discredited in the time domain by means of the Newmark's scheme. The generalized Newmark GN22 method is employed for the displacement field (u, a) as:

$$\begin{bmatrix} \ddot{\overline{\mathbf{u}}}^{t+\Delta t} \\ \ddot{\overline{\mathbf{a}}}^{t+\Delta t} \end{bmatrix} = \begin{bmatrix} \ddot{\overline{\mathbf{u}}}^{t} + ?\,\dddot{\overline{\mathbf{u}}}^{t} \\ \ddot{\overline{\mathbf{a}}}^{t} + ?\,\dddot{\overline{\mathbf{a}}}^{t} \end{bmatrix}$$

$$\begin{bmatrix} \dot{\overline{\mathbf{u}}}^{t+\Delta t} \\ \dot{\overline{\mathbf{a}}}^{t+\Delta t} \end{bmatrix} = \begin{bmatrix} \dot{\overline{\mathbf{u}}}^{t} + \ddot{\overline{\mathbf{u}}}^{t}?\,t + \beta_1 ?\,\dddot{\overline{\mathbf{u}}}^{t}?\,t \\ \dot{\overline{\mathbf{a}}}^{t} + \ddot{\overline{\mathbf{a}}}^{t}?\,t + \beta_1 ?\,\dddot{\overline{\mathbf{a}}}^{t}?\,t \end{bmatrix}$$

$$\begin{bmatrix} \overline{\mathbf{u}}^{t+\Delta t} \\ \overline{\mathbf{a}}^{t+\Delta t} \end{bmatrix} = \begin{bmatrix} \overline{\mathbf{u}}^{t} + \dot{\overline{\mathbf{u}}}^{t}?\,t + \frac{1}{2}\ddot{\overline{\mathbf{u}}}^{t}?\,t^{2} + \frac{1}{2}\beta_2 ?\,\dddot{\overline{\mathbf{u}}}^{t}?\,t^{2} \\ \overline{\mathbf{a}}^{t} + \dot{\overline{\mathbf{a}}}^{t}?\,t + \frac{1}{2}\ddot{\overline{\mathbf{a}}}^{t}?\,t^{2} + \frac{1}{2}\beta_2 ?\,\dddot{\overline{\mathbf{a}}}^{t}?\,t^{2} \end{bmatrix} \tag{10}$$

where $\overline{\beta}$, β_1 and β_2 the Newmark parameters. For unconditional stability of the numerical procedure, it is required that $\overline{\beta} \geq .5$ and $\beta_2 \geq \beta_1 \geq .5$. It must be noted that equation 10 is obtained at the known time t i.e. $\dddot{\overline{\mathbf{u}}}^{t}$, $\ddot{\overline{\mathbf{u}}}^{t}$ and $\overline{\mathbf{u}}^{t}$ are the known values of displacement field. Substituting relation 10 into the space-discrete equation 7, the following nonlinear equation can be achieved.

$$\left[M + .5\,\beta_2 \Delta t^2 K\right] \begin{bmatrix} \Delta\ddot{\bar{u}}^t \\ \Delta\ddot{\bar{a}}^t \end{bmatrix} = [-\Psi] \tag{11}$$

In above equation, $\mathbf{\Psi}$ denotes the vector of known values at time t and $\mathbf{K}$ is the tangential stiffness matrix.

$$\Psi = M\begin{bmatrix} \ddot{\bar{u}}^t \\ \ddot{\bar{a}}^t \end{bmatrix} + K\begin{bmatrix} \bar{u}^t + \dot{\bar{u}}^t \Delta t + .5\ddot{\bar{u}}^t \Delta t^2 \\ \bar{a}^t + \dot{\bar{a}}^t \Delta t + .5\ddot{\bar{a}}^t \Delta t^2 \end{bmatrix} - \left(F\right)^{t+\Delta t} \tag{12}$$

$$K = \frac{d\left(\int_\Omega B^T \sigma d\Omega\right)}{d(u,a)} = \begin{bmatrix} \int_\Omega B^T D\ B\ d\Omega & \int_\Omega B^T D\ B_{Enr} d\Omega \\ \int_\Omega B_{Enr}^T D\ B\ d\Omega & \int_\Omega B_{Enr}^T D\ B_{Enr} d\Omega \end{bmatrix} \tag{13}$$

where D is the appropriate constitutive matrix. The non-linear coupled equation system is linearised in a standard way thus yielding the linear algebraic equation system 11 which can be solved using an appropriate approach, such as the Newton-Raphson procedure.

The Mixed XFEM - Integral Type Nonlocal Formulation: Nonlocal continuum theory uses integral averaging of the variable around its neighborhood, instead of a local definition. For example, nonlocal averaging of plastic strain tensor ($\bar{e}_{ij}^p$) at location x may be defined by the local plastic strain tensor (e_{ij}^p).

$$\bar{\varepsilon}_{ij}^p(x) = \int_V \alpha'(x,\xi)\varepsilon_{ij}^p(\xi)dV \tag{14}$$

where V denotes volume of the body, $\alpha'(\mathbf{x}, \xi)$ is suitable weighting function. In this paper Gaussian distribution function is used as a weighting function.

$$\alpha'(x,\xi) = \frac{e^{-\left(2|\xi - x|/\gamma\right)^2}}{\int_V e^{-\left(2|\zeta - x|/\gamma\right)^2} dV} \tag{15}$$

in which γ is a scalar which is related to material length scale parameter. For numerical finite element computation, the integral definition 14 can be approximated by summation relation. Nonlocal plastic strain tensor can be written as follow:

$$\bar{\varepsilon}_{ij}^p(x) = \sum_k \alpha'(x,x_k)\varepsilon_{ij}^p(x_k) \tag{16}$$

where k denotes gauss points which are closer to point x than 2γ. The value of $\alpha'(\mathbf{x}, \xi)$ for gauss points with greater distance than 2γ is negligible.

In this paper, equation 17 is proposed to calculate the effective stress vector rate from the local and nonlocal plastic strain vector rate.

$$\dot{\sigma} = D^e\dot{\varepsilon} - (1-m)D^e\dot{\varepsilon}^p - mD^e\dot{\bar{\varepsilon}}^p \tag{17}$$

where D^e is linear elastic matrix and m is a constant parameter. Using equation 17, the stress rate at a certain point is related to the plastic strain rate in its neighborhood. If the local plastic strain distribution in a body is smooth, nonlocal plastic strain is approximately equal to local plastic strain; thus, it can be concluded that the proposed formulation is approximately identical to the local formulation. When the distribution of local plastic strain becomes non-smooth, the difference between nonlocal plastic strain and local definition increases and differences between the two formulations are revealed. The formulation presented by Bazant and Lin [11] is a special case of equation 17 where m is considered to be 1; therefore, different patterns for the load-displacement curve can be obtained by changing m. This allows simulation of a wider range of materials. Since the proposed stress-strain relation uses a combination of local and nonlocal plastic strains, this formulation acts as a localization limiter [3]. The value of mE/H in which E denotes the elastic modulus should remain constant during loading to prevent numerical locking. Thus, the model describes the complete loss of material resistance without artificial locking effects.

Since the dissipative energy function is defined in local space, as in classic continuum mechanics, the associated flow rule can be used [3]. As a result, local plastic strain rate is obtained by equation 18.

$$\dot{\varepsilon}^p = \dot{\lambda}\frac{\partial F}{\partial \sigma} \tag{18}$$

where $\dot{\lambda}$ denotes the plastic multiplier and F the yield function which can be defined as: $F(\boldsymbol{\sigma}, \kappa) = f(\boldsymbol{\sigma}) - \kappa = 0$ in which κ is the hardening-softening parameter. Applying the consistency condition to the yield function, $\dot{\lambda}$ can be calculated as:

$$\dot{\lambda} = \frac{\left(\partial F/\partial\sigma\right)^T D^e}{H + \left(\partial F/\partial\sigma\right)^T D^e \left(\partial F/\partial\sigma\right)}\dot{\varepsilon} \tag{19}$$

where H denotes the plastic tangential modulus and is equal to $-(\partial F/\partial\kappa)(\partial\kappa/\partial\boldsymbol{\varepsilon}^p)$. By substituting equations 19 in to 18, vector form of local plastic strain rate is obtained as a function of total strain vector rate.

$$\dot{\varepsilon}^{p}=\frac{\partial F/\partial\sigma\left(\partial F/\partial\sigma\right)^{T}D^{e}}{H+\left(\partial F/\partial\sigma\right)^{T}D^{e}\left(\partial F/\partial\sigma\right)}\dot{\varepsilon}=\Lambda\dot{\varepsilon} \tag{20}$$

By using equations (16), (17) and (20), stress rate at gauss point k can be defined by:

$$\dot{\sigma}_{k}=D_{k}^{e}\left(I-(1-m)\Lambda_{k}\right)\dot{\varepsilon}_{k}-mD_{k}^{e}\left(\sum_{l}\Lambda_{l}\alpha'\left(x_{k},x_{l}\right)\dot{\varepsilon}_{l}\right) \tag{21}$$

where **I** am identity matrix and l denotes gauss points which are closer to gauss point k than 2γ. The tangent stiffness matrix (equation 13) for mixed XFEM-integral type nonlocal plasticity for a specified element can be modified using numerical integration and equation 21.

$$\begin{aligned}\mathbf{K}=&\sum_{k}|J|W_{k}\begin{bmatrix}\boldsymbol{K}_{uu}^{1} & \boldsymbol{K}_{ua}^{1}\\ \boldsymbol{K}_{au}^{1} & \boldsymbol{K}_{aa}^{1}\end{bmatrix}+\ldots\\ &\ldots+\mathrm{m}\sum_{k}|J|W_{k}\begin{bmatrix}\boldsymbol{K}_{uu}^{2} & \boldsymbol{K}_{ua}^{2}\\ \boldsymbol{K}_{au}^{2} & \boldsymbol{K}_{aa}^{2}\end{bmatrix}+\ldots\\ &\ldots-\mathrm{m}\sum_{k}\sum_{l}|J|W_{k}\begin{bmatrix}\boldsymbol{K}_{uu}^{3} & \boldsymbol{K}_{ua}^{3}\\ \boldsymbol{K}_{au}^{3} & \boldsymbol{K}_{aa}^{3}\end{bmatrix}\end{aligned}$$

in which

$$\begin{aligned}&\boldsymbol{K}_{\alpha\beta}^{1}=(\mathbf{B}_{(\mathrm{x_k})}^{\mathrm{T}})^{\alpha}\mathbf{D}_{\mathrm{k}}^{\mathrm{e}}(\mathrm{I}-\mathbf{?}_{\mathrm{k}})(\mathbf{B}_{(\mathrm{x_k})}^{\mathrm{T}})^{\beta} && \boldsymbol{K}_{\alpha\beta}^{2}=(\mathbf{B}_{(\mathrm{x_k})}^{\mathrm{T}})^{\alpha}\mathbf{D}_{\mathrm{k}}^{\mathrm{e}}(\mathbf{?}_{\mathrm{k}})(\mathbf{B}_{(\mathrm{x_k})}^{\mathrm{T}})^{\beta}\\ &\boldsymbol{K}_{\alpha\beta}^{3}=(\mathbf{B}_{(\mathrm{x_k})}^{\mathrm{T}})^{\alpha}\mathbf{D}_{\mathrm{k}}^{\mathrm{e}}(\mathbf{?}_{\mathrm{k}})\mathrm{a}'\left(\mathbf{x}_{\mathrm{k}},\mathbf{x}_{l}\right)(\mathbf{B}_{(\mathrm{x_k})}^{\mathrm{T}})^{\beta} && (\mathbf{B}_{(\mathrm{x_k})})^{u}=\mathbf{B}_{(\mathrm{x_k})},(\mathbf{B}_{(\mathrm{x_k})})^{a}=\mathbf{B}_{(\mathrm{x_k})\mathrm{Enr}}\end{aligned} \tag{22}$$

where $|J|$ is determinant of Jacobian matrix and W_k denotes weight coefficient of the gaussian quadrature. If the second and third terms in equation 22 are ignored, the formulation becomes equivalent to local theory. The DOF of one element may become related to the DOF of a non-neighboring element because of the third term of equation 22. In conclusion, the nonzero components of the tangent stiffness matrix increase. In this situation, the tangent stiffness matrix is not symmetrical because $\alpha'(\mathbf{x}_k, \mathbf{x}_l) \neq \alpha'(\mathbf{x}_l, \mathbf{x}_k)$.

Determination of Strain Localization Interface: By applying enrichment functions to the formulation, additional DOF must be assigned to the nodes. At the beginning of the analysis, the additional DOF are inactive. For this reason a criterion must be defined for the activation of additional DOF. This study proposed the local bifurcation criterion to locate strain localization interface. In the case of a symmetric constitutive model, this criterion coincides with the singularity of the acoustic tensor. Acoustic tensor can be defined as:

$$A_{ij}=C^{ep}{}_{ikjl}n_{k}\,n_{l} \tag{23}$$

where n is a unit vector and $C^{ep}{}_{ikjl}$ denotes local elastoplastic constitutive tensor.

$$C_{ikjl}^{ep}=C_{ikjl}^{e}-\frac{C_{ikmn}^{e}\,\partial F/\partial\sigma_{mn}C_{pqjl}^{e}\,\partial F/\partial\sigma_{pq}}{\left(H+\partial F/\partial\sigma_{rs}C_{rstu}^{e}\,\partial F/\partial\sigma_{tu}\right)} \tag{24}$$

If there is a direction in which the determinant of the acoustic tensor becomes zero or negative, strain localization probably starts and XFEM must be used to approximate the displacement field. At each Gauss point, then, a direction must be found in which the determinant of the acoustic tensor has the lowest value. One independent variable is sufficient to describe unit vector n in two-dimensional space. As a result, the determinant of the acoustic tensor is a function of one variable and its lowest value can easily be calculated. This approach allows us to identify points where strain localization is likely to occur.

In order to perform the numerical algorithm, it is assumed that the interface, i.e. the centerline of the localization zone and the Gauss points which have a negative determinant of the acoustic tensor are known at time t (Fig. 2). Moreover, the vector V corresponding to the minimum determinant of the acoustic tensor at the last point of the interface, i.e. L, is known at time t.

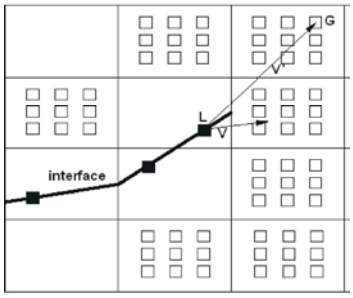

Fig. 2: Computational algorithm for the localization interface growth at step *n*

The vector V' is plotted from L to the Gauss point which has a negative determinant of the acoustic tensor, i.e. G. Then the angle between V and V' is obtained. The next point for the centerline of the localization zone is a Gauss point whose corresponding vector V' has a minimum angle with V. Once the new interface is detected, additional DOF are activated at every nodal point whose support has an intersection with the enriched zone. If convergence is obtained at the end of the increment, the evolution of shear band is carried out to obtain the new interface for the next loading step. This technique is simple and has been employed in the examples. To avoid doubling back on the original path, the angle between the pieces of strain localization interface must be less than 90 degrees.

Numerical Simulation: In order to demonstrate a part of the wide range of problems that can be solved by the present approach, we have illustrated the effective performance of XFEM technique using the integral type nonlocal continuum in strain localization analysis. A computer program has been developed to investigate the computational aspects of the XFEM model in a higher order continuum model. Several numerical simulations, including one dimensional tension bar, a strip in tension and the vertical slope problem have been presented to illustrate the performance and efficiency of the proposed formulation. The finite element mesh employed in all simulations was eight-noded rectangular and six-noded triangular plane strain elements with nine and seven integration points, respectively. The analysis starts with the standard FE model with no enrichment functions. The enrichment function is then implemented into the standard shape functions by tracing the evolution of shear band zone. The parameter β, which is defined the width of enrichment zone, is set to γ in all analyzes due to the fact that the shear band thickness is about γ. All elements closer to the strain localization interface than β are enriched by the hyperbolic tangent function.

For integration purposes, a decomposition of the elements into sub-elements that align with the interface is standard in the XFEM [21]. In the case of a rectangular element, the elements located on the interface were partitioned using triangular sub-elements (Fig. 3a) and 24 Gauss quadrature points were used for the elements cut by the shear band interface. For standard FE elements, a set of 3×3 Gauss points were used for numerical integration. If an interface surface was added during the evolution of the shear band zone (Fig. 3b), the number of Gauss quadrature points for an element may differ before and after each increment. In this case, the value of the stresses can be determined at the standard FE Gauss points of an element. To obtain these values at the Gauss quadrature points of sub-triangles, a simple interpolation on a support domain for each triangular Gauss point consisting of the three nearest standard FE Gauss points was used. The required stress value can be determined using a simple interpolation.

One Dimensional Tension Bar: In the first example, the efficiency of the proposed integral type nonlocal plasticity was investigated. The local and nonlocal strain-softening plasticity were used with material parameters pertinent to the von-Mises yield criterion. Constitutive model parameters and boundary condition are shown in Fig. 4. Weak zone was considered in the central part of the bar. The initial yield stress of this zone was assumed be equal to 99 percent of the initial yield stress in other parts of the bar. As a result, the strain localization initiated from the center as shown in Fig. 4 by the shaded area. The parameter γ was set to 1.4cm and *m* was set to 2 to obtain the band width equal to 3.5 cm. The loading was applied incrementally with a displacement control method. The bar was divided into 7, 15 and 31 elements to examine the mesh dependency of local and integral type nonlocal plasticity.

The stress-equilibrium condition implies that the stress must be constant across the entire bar. The stress in the bar initially increases linearly with applied displacement $\Delta\delta$. After the stress reaches its peak, strain localization is initiated from the bar center. In the framework of local plasticity, the bar is in a loading state inside the central element and an unloading state outside it. Due to softening inside the band, the stress in the bar decreases. The softening zone width becomes narrower as the mesh is refined, so the global load–displacement curve becomes mesh sensitive. The plastic strain distributions along the bar and load–displacement curve are shown in Fig. 5 and 6 respectively. As seen, snap back phenomenon occurs in the medium and fine mesh.

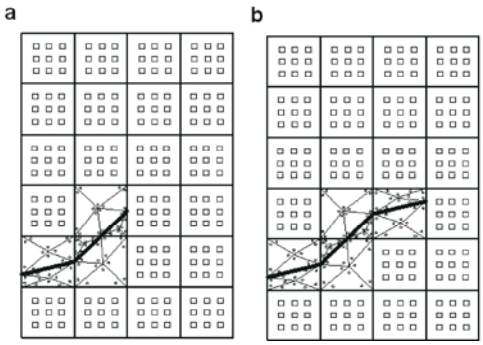

Fig. 3: Modeling of localization interface in XFEM; (a) The sub-triangles associated with elements cut by the interface at step n, (b) the sub-triangles obtained by partitioning procedure at step n + 1

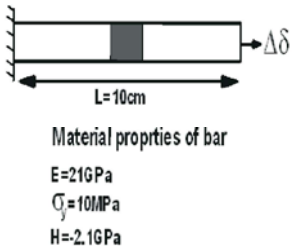

Fig. 4: One-dimensional tension bar (Constitutive model parameters and boundary condition)

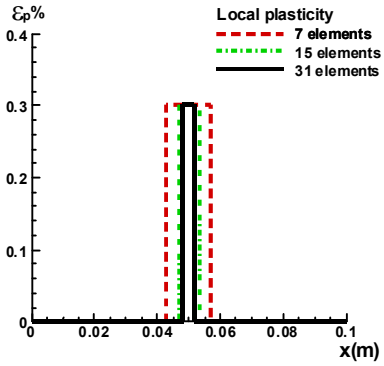

Fig. 5: Plastic strain distribution from the local plasticity

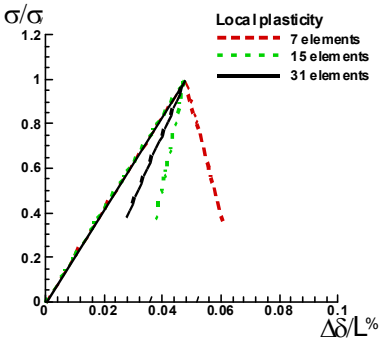

Fig. 6: Load–displacement responses from the local plasticity

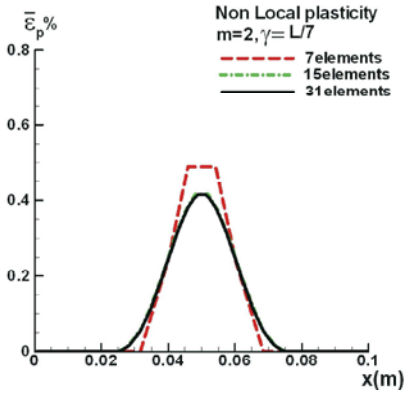

Fig. 7: Non-local Plastic strain distributions from the proposed nonlocal plasticity

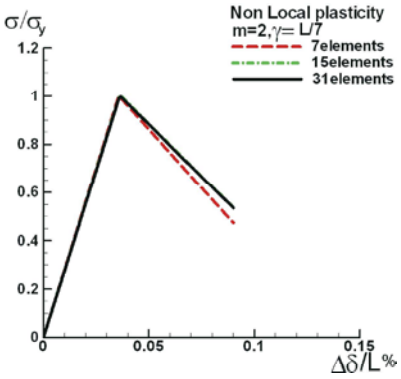

Fig. 8: Load–displacement responses from the proposed nonlocal plasticity

As shown in Fig. 7, by using the proposed integral type nonlocal plasticity model, the bandwidth and nonlocal plastic strain distribution remain almost identical for different meshes and the load–displacement responses display very slight differences in the three meshes (Fig. 8). In the proposed nonlocal plasticity, when the mesh is refined, more elements are involved in defining a plastic zone of constant size. The range of elements that are in a loading state are determined by γ which is a function of material length scale parameter.

Plane Strain Strip in Tension: In the second example, simulation was done in the frame work of mixed XFEM-integral type nonlocal plasticity with strain softening. Geometry, boundary condition and material parameters are shown in Fig. 9. The strip was restrained at the bottom edge in the vertical direction and a uniform vertical displacement was imposed on the upper nodes while the other two degrees-of-freedom were set free. In order to avoid the homogeneous solution, the shaded area of the strip was taken as the weak zone, as shown in Fig. 9. If the localization condition happens, this part will

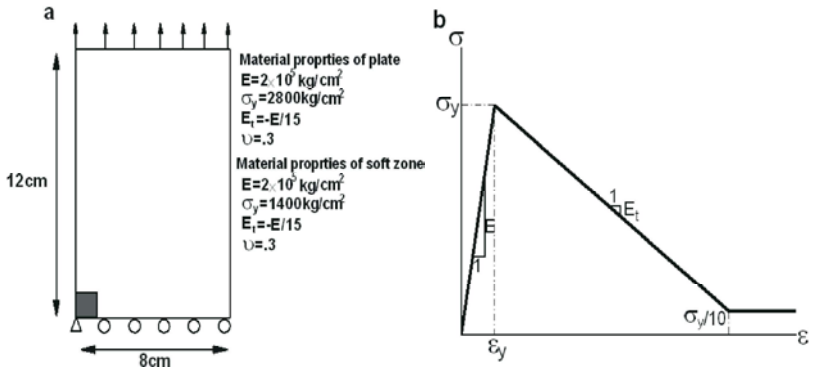

Fig. 9: The plane strain strip in tension; (a) The geometry, boundary conditions and material properties, (b) the stress-strain curve

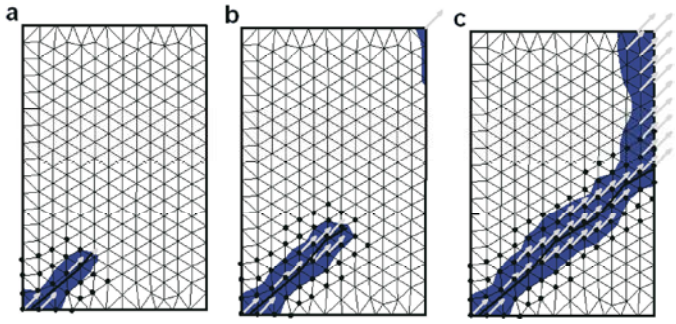

Fig. 10: The evolution of strain localization interface , negative determinant of acoustic tensor contour and vectors corresponding to the minimum determinant of acoustic tensor for the strip in tension; (a) $\Delta\delta$=.165cm (b) $\Delta\delta$=.169cm (c) $\Delta\delta$=.172cm

be the first region that triggers localization. The von-Mises yield criterion with a bilinear stress–strain-softening curve was used. The parameter γ was set to 1cm and m was set to .8 to obtain the shear band thickness equal to 1.3 cm.

Growth of the strain localization interface in each step was determined by local bifurcation criterion. Fig. 10 presents the evolution of strain localization interface together with the enriched nodes, negative determinant of the acoustic tensor contour and vectors corresponding to the minimum determinant of acoustic tensor at three different steps. At the end of simulation, the total numbers of 77 additional DOF have been added to the system. Fig. 11 presents the deformed configuration for different deformations, i.e. $\Delta\delta$=.4, .8 and 1.2 cm. In Fig. 12, the nonlocal effective plastic strain contours are presented for the mixed XFEM-integral type nonlocal analysis at three mesh movements. It can be observed that this technique gives a clear picture of the failure. In order to illustrate the efficiency and accuracy of the proposed algorithm, the mixed XFEM-integral type nonlocal analysis were compared with an adaptive FEM simulation based on the Cosserat theory reported in reference [27]. In the mixed XFEM-integral type nonlocal model, 430 elements were used while in the adaptive FEM analysis, 1166 elements were used in simulation. Therefore, the XFEM method is a numerical method that can be applied to decrease the required mesh density close to the shear band. In Fig. 13, the strip reaction versus prescribed displacement is shown for the XFEM technique using the hyperbolic tangent function and an adaptive FEM analysis. There is a good agreement between two different techniques. This example clearly presents the efficiency of the mixed XFEM-integral type nonlocal model even with a uniform coarse mesh.

The change of inclination (α) and thickness (t) of the shear band with increases of m and γ are shown in Fig. 14 and 15. The thickness of the shear band increased while inclination of the shear band decreased as m and γ increased. Moreover, the maximum value of the nonlocal effective plastic strain decreased with the increase of m and γ. Strip reaction versus prescribed displacement is shown for m = 0.6, 1, 1.5, 3 and γ =0.6, 1, 1.5, 3 in Fig. 16. The effect of m and γ can be observed in the force–displacement curve. Up to the peak, all curves coincide. Obviously, the nonlocal term first influenced the results when localization occurred. Thereafter, the amount of softening depended on the value of m and γ.

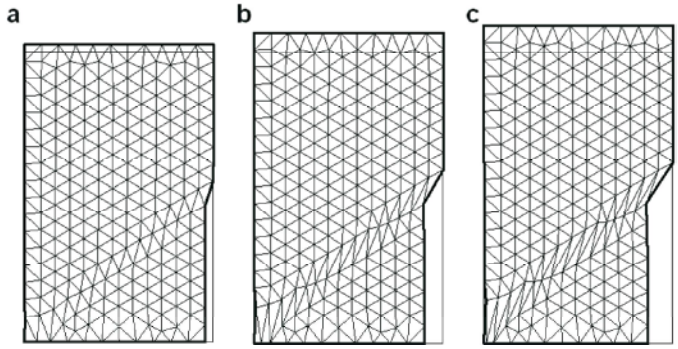

Fig. 11: The deformed mesh for the strip in tension at different deformations; (a) Δδ=.4cm (b) Δδ=.8cm (c) Δδ=1.2cm

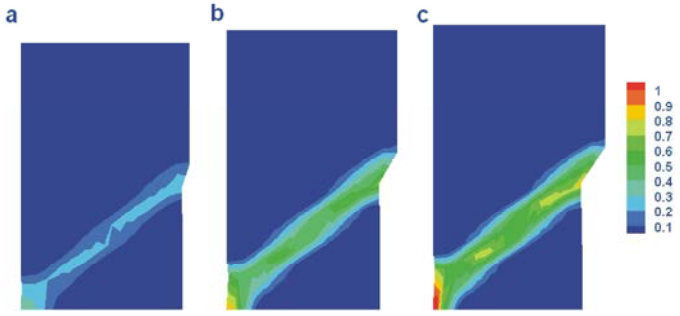

Fig. 12: The nonlocal effective plastic strain contours for the strip in tension at different deformations; (a) Δδ=.4cm (b) Δδ=.8cm (c) Δδ=1.2cm

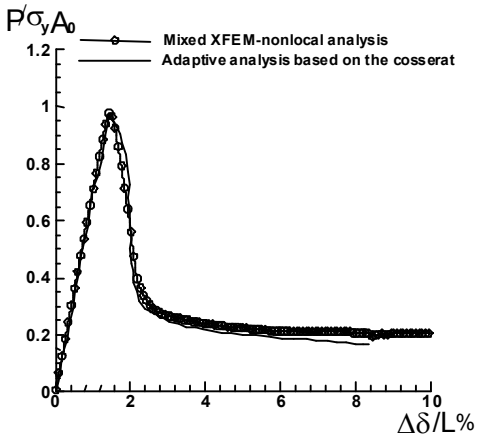

Fig. 13: The variation of the strip reaction with prescribed displacement; a comparison between the adaptive FEM and mixed XFEM-nonlocal methods

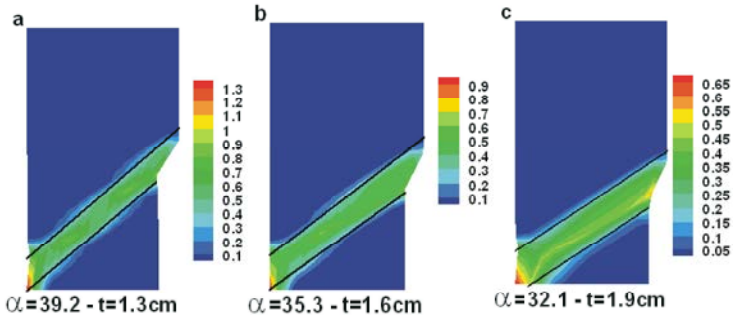

Fig. 14: Inclination and thickness of the shear band for different value of *m* a) *m*=0.6 b) *m*=1.5 c) *m*=3

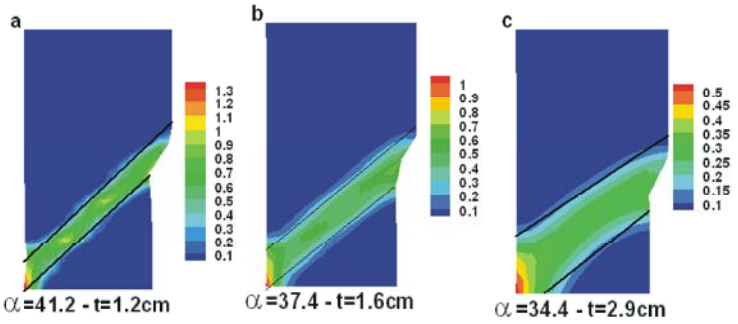

Fig. 15: Inclination and thickness of the shear band for different value of γ a) γ=.6cm b) γ=1.5cm c) γ=3cm

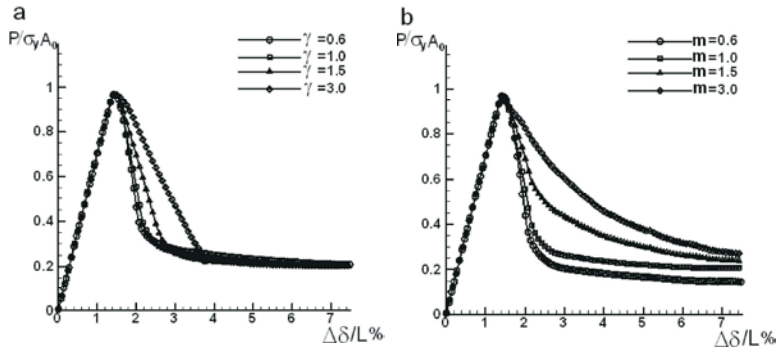

Fig. 16: The variation of the strip reaction with prescribed displacement; (a) the effect of γ (b) the effect of m

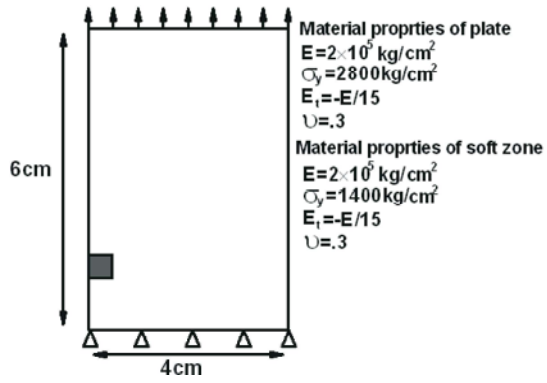

Fig. 17: The plane strain strip in tension; The geometry, boundary conditions and material properties

Higher values of m resulted in less softening. Residual reaction force increased with increasing of m and did not change with increasing of γ. Thus, different load-displacement curves can be obtained by changing m and γ.

Comparison of the Nonlocal and Mixed XFEM-Nonlocal Model: In this example, the performance of the nonlocal formulation and mixed nonlocal-XFEM formulation were compared. The geometry, boundary conditions and material parameters are shown in Fig. 17. The strip was restrained at the bottom edge in the vertical and horizontal direction and a uniform vertical displacement was imposed on the upper nodes. The stress–strain curve as for the previous example was considered. The shaded area in Fig. 17 represents the weak inclusion. The weak inclusion was introduced to trigger the localization. The parameter γ was set to 1cm and m was set to 1.5 to obtain the shear band thickness equal to 1.3 cm. In order to show the capability of the nonlocal extension with XFEM, numerical results obtained using different meshes are presented. The meshes consisted of 96, 384 and 651 four-node.

The results of the nonlocal and mixed XFEM-nonlocal formulation are shown in Fig. 18-21. Fig. 18 and 20 present the deformed configuration and Fig. 19 and 21 present the nonlocal effective plastic strain contours for both formulations. As seen in Fig. 18 and 19, the results for coarse mesh are different than for other mesh results in the nonlocal formulation. In the proposed approach, good agreement can be observed between the three mesh sizes; therefore, the XFEM can be applied to the problem to decrease the required mesh density close to the of the localization band (Fig. 20 and 21). These figures confirm that mixed XFEM-nonlocal technique gives good prediction of localization even for the coarse mesh.

In the case of coarse mesh size, some amount of plastic strain was created in the near top right corner of the strip in nonlocal analysis and plastic strain was

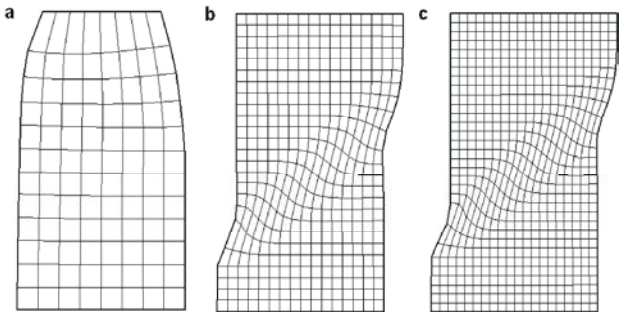

Fig. 18: The deformed mesh from nonlocal model; a) coarse mesh b)medium mesh c) fine mesh

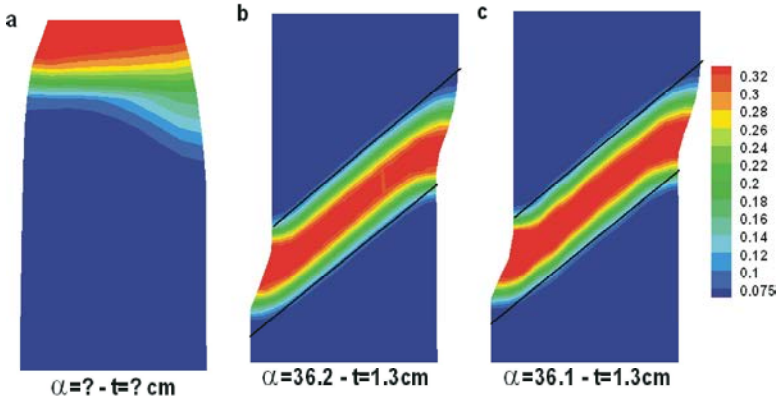

Fig. 19: The effective plastic strain contour, inclination and thickness of the shear band from nonlocal model; a) coarse mesh b)medium mesh c) fine mesh

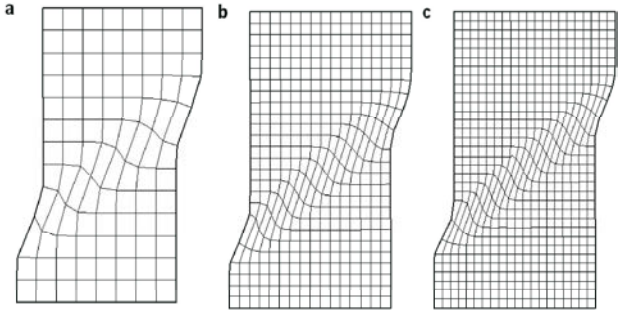

Fig. 20: The deformed mesh from mixed XFEM-nonlocal model; a) coarse mesh b)medium mesh c) fine mesh

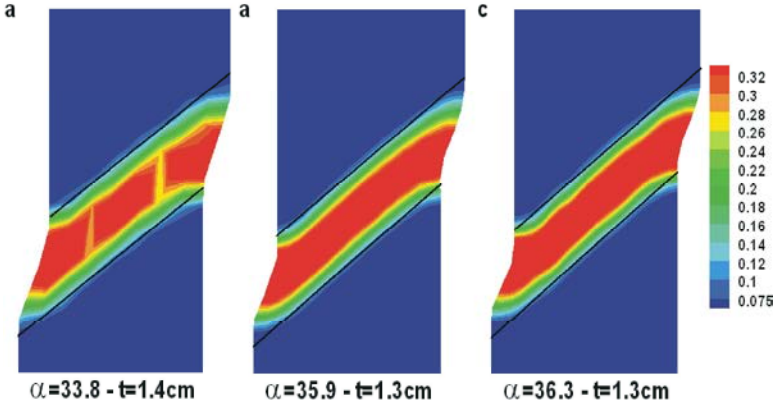

Fig. 21: The effective plastic strain contour, inclination and thickness of the shear band from mixed XFEM-nonlocal model; a) coarse mesh b)medium mesh c) fine mesh

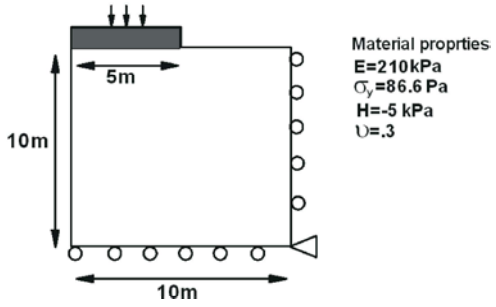

Fig. 22: Elastoplastic softening material, geometry and boundary conditions for a vertical slope

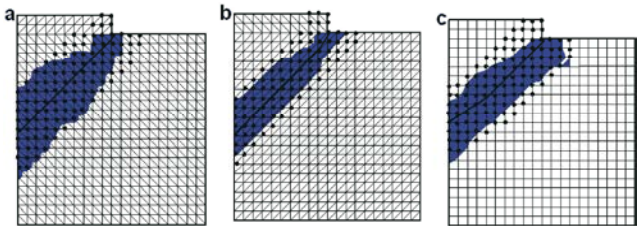

Fig. 23: The strain localization interface and negative determinant of acoustic tensor contour for the vertical cut at Δδ=0.5cm; (a) triangular 'bad mesh' (b) triangular 'good mesh' (c) quadrilateral 'uniform mesh'

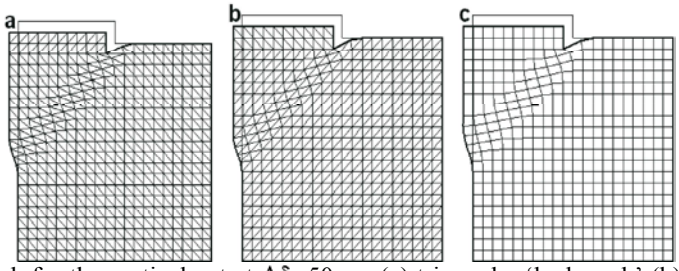

Fig. 24: The deformed mesh for the vertical cut at Δδ=50cm; (a) triangular 'bad mesh' (b) triangular 'good mesh' (c) quadrilateral 'uniform mesh'

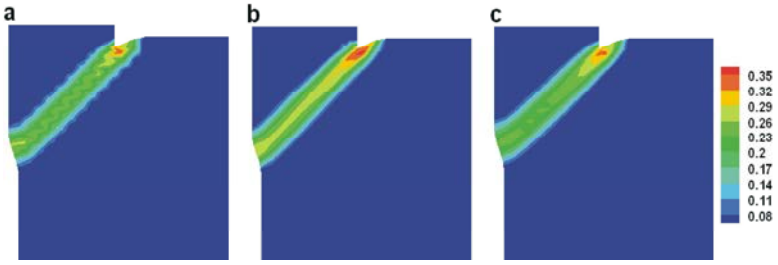

Fig. 25: The nonlocal effective plastic strain contours for the vertical cut at Δδ=50cm; (a) triangular 'bad mesh' (b) triangular 'good mesh' (c) quadrilateral 'uniform mesh'

attracted by the boundary. Therefore, failure pattern was not predicted correctly by nonlocal formulation. In the mixed XFEM-nonlocal analysis, gradient of displacement and plastic strain on the localization interface was greater than other points because of the enrichment function. Therefore, mixed XFEM-nonlocal technique gives good prediction of localization even for the coarse mesh.

Thickness and inclination of the shear band for three different meshes are shown in Fig. 19 and 21. As seen, there is a good agreement between the results for different meshes i.e. the width and inclination of the shear band are independent of the element size.

Vertical Slope Problem: The next example is of a vertical slope with a rigid footing resting on its crest. The parameters of constitutive model and boundary conditions are shown in Fig. 22. The rigid footings have been assumed to be elastic, with an elastic modulus 100 times higher than that of the soil. The vertical slope was analyzed for three meshes; triangular 'bad mesh',

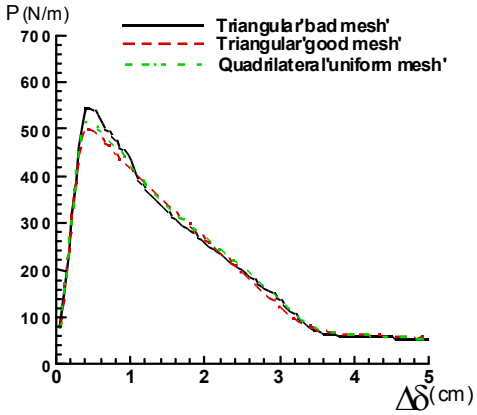

Fig. 26: The variation of the vertical slope reaction with prescribed displacement for different meshes

triangular 'good mesh' and quadrilateral 'uniform mesh'. This example was chosen to show that the mixed XFEM-integral type nonlocal model can give good results even with bad mesh and different mesh alignments. The present problems have been solved with displacement control by increasing the footing settlement in an incremental manner. γ and m were taken equal to 1m and 1.5 respectively. The strain localization interfaces together with the enriched nodes and negative determinant of acoustic tensor contours at $\Delta\delta$=0.5cm are shown in Fig. 23. In Fig. 24 and 25, the deformed mesh configurations and the nonlocal effective plastic strain contours are presented at $\Delta\delta$=50cm. Clearly, the finite width of the localization band and its independency of the finite element size can be observed in these Figs. Fig. 26 shows the load deflection curves for three different meshes. The results display that the reaction become close between these three meshes.

CONCLUSION

In the present study, an enriched finite element technique was employed based on an integral-type nonlocal theory for simulation of strain localization. The governing equations were regularized using nonlocal averaging of the plastic strain tensor, which included the material length scale parameter. The nonlocal model of Bazant and Lin [11] was extended. The efficiency of the proposed nonlocal model was demonstrated by simulation of one dimensional tension bar. Approximation of the displacement field in the localization band was improved by incorporating a set of special enrichments. The tangent stiffness matrix was derived for the mixed XFEM-integral type nonlocal formulation. Standard FE analysis was first employed with no enrichment functions to perform the numerical simulation. The enrichment functions were then incorporated into the standard shape functions after the evolution of the localization band. A new method based on the local bifurcation theory was proposed for the initiation and growth criterion of the strain localization interface. When using this method, the softening zone initiation locus did not need to be known in advance. Finally, several numerical examples, including one dimensional tension bar, a strip in tension and the vertical slope problem, were analyzed to demonstrate the efficiency of the combined XFEM–integral type nonlocal continuum model in simulation of strain localization. It was shown that the proposed computational algorithm is able to accurately capture the evolution of strain localization with local bifurcation criterion and XFEM without mesh dependency problems. The effect of the internal length parameter on the thickness and inclination of the shear band was investigated. It was shown that the nonlocal model preserved the well-posedness of the governing equations in the post-localization regime and prevented pathological mesh sensitivity of the numerical results if the size of the element was smaller than $\gamma/2$. The mixed XFEM-nonlocal model guaranteed mesh independence even if the size of the elements was larger than $\gamma/2$. In the other words, coarser mesh can be used for XFEM combined with a nonlocal model than when using only a nonlocal model. The computational effort required for the mixed XFEM-nonlocal model was less than for the nonlocal formulation because coarser mesh can be used in simulation. For the mixed XFEM-nonlocal model, the width and inclination of the shear band was obtained independently of element size. Mesh alignment was also investigated for the vertical cut. The results were almost invariant to the influence of mesh alignment.

REFERENCES

1. Borst De, R., L.J. Sluys, H.B. Muhlhaus and J. Pamin, 1993. Fundamental issues in finite element analyses of localization of deformation. Engineering Computations, 10(2): 99-121.
2. Sulem, J. and I. Vardoulakis, 1995. Bifurcation Analysis in Geomechanics. Blackie Academic and Professional, pp: 462.
3. Jirasek, M. and S. Rolshoven, 2003. Comparison of integral-type nonlocal plasticity models for strain softening materials. International Journal of Engineering Science, 41(13): 1553-1602.

4. Tejchman, J., 2002. Patterns of shear zones in granular materials within a polar hypoplastic continuum. Acta Mechanica, 155(1-2): 71-95.
5. Borst De, R. and H.B. Muhlhaus, 1992. Gradient dependent plasticity: formulation and algorithmic aspects. International Journal for Numerical Methods in Engineering, 35(3): 521-539.
6. Loret, B. and J.H. Prevost, 1990. Dynamic strain localisation in elasto(visco-)plastic solids. Part 1. General formulation and one-dimensional examples. Computer Methods in Applied Mechanics and Engineering, 83(3): 247-273.
7. Tejchman, J., 2003. A non-local hypoplastic constitutive law to describe shear localisation in granular bodies. Archives of Hydro-Engineering and Environmental Mechanics, 50(4): 229-250.
8. Eringen, A.C., 1981. On nonlocal plasticity. International Journal of Engineering Science, 19(12): 1461-1474.
9. Eringen, A.C., 1983. Theories of nonlocal plasticity. International Journal of Engineering Science, 21(7): 741-751.
10. Pijaudier-Cabot, G. and Z.P. Bazant, 1987. Nonlocal damage theory. Journal of Engineering Mechanics, 113(10): 1512-1533.
11. Bazant, Z.P. and F.B. Lin, 1988. Nonlocal yield-limit degradation. International Journal for Numerical Methods in Engineering, 26(8): 1805-1823.
12. Stromberg, L. and M. Ristinmaa, 1996. FE-formulation of a nonlocal plasticity theory. Computer Methods in Applied Mechanics and Engineering, 136(1-2): 127-144.
13. Brunig, M., S. Ricci and H. Obrecht, 2001. Nonlocal large deformation and localization behavior in metals. Computers and Structures, 79(22-25): 2063-2074.
14. Maier, T.H., 2003. Nonlocal modeling of softening in hypoplasticity. Computers and Geotechnics, 30(7): 599-610.
15. Maier, T., 2004. Comparison of non-local and polar modelling of softening in hypoplasticity. International Journal for Numerical and Analytical Methods in Geomechanics, 28(3): 251-268.
16. Tejchman, J., 2004. Comparative FE-studies of shear localizations in granular bodies within a polar and non-local hypoplasticity. Mechanics Research Communications, 31(3): 341-354.
17. Jirasek, M., 1998. Nonlocal models for damage and fracture comparison of approaches. International Journal of Solids and Structures, 35(31-32): 4133-4145.
18. Bazant, Z.P. and M. Jirasek, 2002. Nonlocal integral formulations of plasticity and damage survey of progress. Journal of Engineering Mechanics, 128(11): 1119-1149.
19. Melenk, J.M. and I. Babuska, 1996. The Partition of Unity Finite Element Method: Basic Theory and Applications. Computer Methods in Applied Mechanics and Engineering, 139(1): 289-314.
20. Belytschko, T. and T. Black, 1999. Elastic crack growth in finite elements with minimal remeshing. International Journal for Numerical Methods in Engineering, 45(5): 601-620.
21. Fries, T.P. and T. Belytschko, 2010. The extended/generalized finite element method: an overview of the method and its applications. International Journal for Numerical Methods in Engineering, 84(3): 253-304.
22. Patzak, B. and M. Jirasek, 2003. Process zone resolution by extended finite elements. Engineering Fracture Mechanics, 70(7): 957-977.
23. Samaniego, E. and T. Belytschko, 2005. Continuum-discontinuum modelling of shear bands. International Journal for Numerical Methods in Engineering, 62(13): 1857-1872.
24. Areias, P.M.A. and T. Belytschko, 2006. Two-scale shear band evolution by local partition of unity. International Journal for Numerical Methods in Engineering, 66(5): 878-910.
25. Song, J.H., P.M.A. Areias and T. Belytschko, 2006. A method for dynamic crack and shear band propagation with phantom nodes. International Journal for Numerical Methods in Engineering, 67(6): 868-893.
26. Areias, P.M.A. and T. Belytschko, 2007. Two-scale method for shear bands: thermal effects and variable bandwidth. International Journal for Numerical Methods in Engineering, 72(6): 658-696.
27. Khoei, A.R. and K. Karimi, 2008. An enriched-FEM model for simulation of localization phenomenon in Cosserat continuum theory. Computational Materials Science, 44(2): 733-749.
28. Jirasek, M. and B. Patzak, 2000. Adaptive technique for nonlocal models. In the Proceedings of the ECCOMAS.
29. Bigoni, D. and T. Hueckel, 1991. Uniqueness and localization - I: associative and nonassociative elastoplasticity. International Journal of Solids and Structures, 28(2): 197-213.
30. Hill, R., 1962. Acceleration waves in solids. Journal of the Mechanics and Physics of Solids, 10(1): 1-16.

31. Rice, J.R., 1976. The localization of plastic deformation. In the Proceedings of the Theoretical and Applied Mechanics, pp: 207-220.
32. Benallal, A. and C. Comi, 2003. Perturbation growth and localization in fluid saturated inelastic porous media under quasi-static loadings. Journal of the Mechanics and Physics of Solids, 51(5): 851-899.
33. Bésuelle, P. and R. Chambon, 2006. Modelling the post-localization regime with local second gradient models non uniqueness of solutions and non persistent shear bands. In the Proceedings of the Modern Trends in Geomechanics, pp: 209-221.
34. Andrade, J.E. and R.I. Borja, 2007. Modeling deformation banding in dense and loose fluid saturated sands. Finite Elements in Analysis and Design, 43(5): 361-383.